Acta Astronautica 200 (2022) 435–447

Contents lists available at ScienceDirect

Acta Astronautica

journal homepage: www.elsevier.com/locate/actaastro

Research paper

In silico study of the posture-dependent cardiovascular performance during parabolic flights

Matteo Fois [a,*], Luca Ridolfi [b], Stefania Scarsoglio [a]

[a] Department of Mechanical and Aerospace Engineering, Politecnico di Torino, Corso Duca degli Abruzzi 24, Turin 10129, Italy
[b] Department of Environmental, Land and Infrastructure Engineering, Politecnico di Torino, Corso Duca degli Abruzzi 24, Turin 10129, Italy

ARTICLE INFO

Keywords:
Computational hemodynamics
Multiscale cardiovascular modeling
Parabolic flight
Bioastronautics
Cardiac performance
Intracranial pressure

ABSTRACT

Space exploration plays a crucial role in research and technological advance. Yet, weightlessness entails severe risks for human life that are investigated through both Earth-based and on-orbit experiments. To this aim, parabolic flights are used to study the short-term response of the human cardiovascular system (*CVS*) to micro- (~0 g) and hypergravity (up to 1.8 g). However, the short flight duration and technical difficulties associated with invasive *in vivo* measurements allow for the acquisition of a very limited number of hemodynamic variables. To enrich the picture, numerical tools can represent a powerful alternative. In this work, a new validated multiscale model of the *CVS* is proposed to inquire into global and central hemodynamic alterations – including cardiac mechano-energetic balance – triggered by parabolic flight at different postures (supine, seated and standing). Our analyses show that: (i) gravity-induced *CVS* changes strongly depend on posture; (ii) central aortic pressure, cardiac work and oxygen consumption indexes are significantly influenced by blood migration between central and lower body regions elicited by gravity variation; and (iii) cardiac efficiency improves during 20 s microgravity, while worsening in both hypergravity phases. Finally, (iv) the role of mildly elevated intracranial pressure (*ICP*) encountered in 0 g is discussed as a potential risk factor for spaceflight-induced visual impairment.

1. Introduction

Spaceflights and interplanetary explorations have always aroused enormous fascination and interest in mankind, and in recent decades they are becoming more and more accessible. Unfortunately, still little is known concerning human adaptation to the space environment, although multiple risks and life-threatening consequences (*i.e.*, bone mass loss, osteoporosis, radiation exposure, muscular atrophy) have been revealed by recent studies for missions lasting up to six months [1–5]. Among different ground analogs of microgravity conditions (head-down tilt, water immersion, drop towers, etc. [3]), parabolic flights are the only ones where actual free-falling – albeit of limited duration – is reproduced on passengers. This is possible due to the almost complete body gravity unloading experienced at the apex of the parabolic trajectory followed during a parabolic flight, which is performed 20–30 times for each experimental campaign. Differently, water immersion and head-down bed rest produce only virtual gravity unloading, either by aligning the body axis perpendicularly to the gravity vector, or due to the pulling action exerted by the liquid, whereas drop towers experiments are definitely unfeasible. Therefore, parabolic flights represent the cheapest and most affordable Earth analog of actual spaceflight in mimicking short-term microgravity occurrence on humans. For each parabola, the subjects undergo a sequence of short-term exposure to hypergravity (after the pull-up from 1 g to 1.8 g), followed by microgravity (~0 g) and a second hypergravity (with subsequent pull-out from 1.8 g to 1 g) phases, lasting about 20 s each, including transitions. Therefore, the spurious influence of the pre- and post-0 g hypergravity phases should be taken into consideration when analyzing the subjects response to acute microgravity.

In past years, a conspicuous number of parabolic flight campaigns were promoted with the purpose of collecting information about the human physiological systems coping with reduced gravity. In particular, the role of the cardiovascular system (*CVS*[1]) was explored, even though only simple and, in most cases, non-invasive *in vivo* measurements were acquired (*e.g.* heart rate, finger or brachial arterial pressure). Most authors focused on single phase-averaged responses of main hemodynamic variables [6–11], though some reported also continuous monitoring of the investigated parameters [12–14]. In [6], the authors provided a detailed analysis on the role of posture in the

* Corresponding author.
E-mail address: matteo.fois@polito.it (M. Fois).
[1] See Nomenclature.

https://doi.org/10.1016/j.actaastro.2022.08.018
Received 31 March 2022; Received in revised form 17 June 2022; Accepted 8 August 2022
Available online 27 August 2022

Nomenclature

α	Tilt angle
$\widehat{EI}$	Carotids flexural rigidity
ρ	Blood density
Δh_{H-jv}	Head-jugular vein anatomical distance
Δh_{H-ra}	Head-right vertical anatomical distance
Δp^{h}_{H-jv}	Head-jugular vein hydrostatic pressure difference
Δp^{h}_{H-ra}	Head-right atrium hydrostatic pressure difference
A	Vessels cross-section area
A_b	Carotids buckling cross-section area
A_{dia}	Diastolic portion of the aortic pressure waveform area
A_{sys}	Systolic portion of the aortic pressure waveform area
B_i	Vessels mechanical coefficients
$cMAP$	Central arterial pressure (aorta)
CO	Cardiac output
CVP	Central venous pressure
CVP_{sup}	Central venous pressure at supine posture
CVP_{tilt}	Central venous pressure at tilted posture
CVS	Cardiovascular system
C	Vessels compliance
DAP	Diastolic arterial pressure (peripheral)
EF	Ejection fraction
g_0	Baseline (Earth) gravity acceleration
g	Gravity acceleration
HR	Heart rate
ICP	Intracranial pressure
ICP_{sup}	Intracranial pressure at supine posture
ICP_{tilt}	Intracranial pressure at tilted posture
IMP	Intramyocardial pressure
IOP	Intraocular pressure
ITP	Intrathoracic pressure
la	Left atrium
lv	Left ventricle
L	Blood inertia or inertance
MAP	Mean arterial pressure (peripheral)
n	degree of curvature of the carotid $p-A$ hyperbolic relationship
pa	Pulmonary arteries
PE	Left ventricle potential energy
PVA/min	Pressure–volume area per minute
PVA	Pressure–volume area
pv	Pulmonary veins
p	Blood pressure
p_b	Carotids buckling pressure
p_{lved}	Left ventricle end-diastolic pressure
p_{lves}	Left ventricle end-systolic pressure
Q	Blood flow rate
ra	Right atrium
RPP	Rate-pressure product
RR	Heartbeat duration
rv	Right ventricle
R	Vessels hydraulic resistance
$SANS$	Spaceflight-associated neuro-ocular syndrome
SAP	Systolic arterial pressure (peripheral)
SV	Stroke volume
SW/min	Stroke work per minute
SW	Stroke work
TPR	Total peripheral resistance
TTI/min	Tension-time index per minute
TTI	Tension-time index
t	Time
V	Blood volume
V^{un}_{lv}	Left ventricle unstressed volume
V_{cp}	Cardiopulmonary blood volume
V_{lved}	Left ventricle end-diastolic volume
V_{lves}	Left ventricle end-systolic volume
x	Vessels axial coordinate

hemodynamic response to parabolic flight, whereas in other works different aspects were explored, such as post-flight induced orthostatic intolerance [15], the impact of the Valsalva maneuver [16] or the particular response to different reduced-gravity environments (*e.g.*, Moon, Mars) [17,18]. Only few studies [14,19] reported data from (non-invasive) estimation of central aortic pressure, obtained by transfer function reconstruction. Yet, comprehension of central (aortic and cardiac) hemodynamics is crucial to adequately assess the actual *CVS* response to weightlessness. For instance, catheterized monitoring of central venous pressure (*CVP*) during a parabolic flight campaign showed fundamental discrepancies with respect to other ground experiments often considered as analogs of microgravity conditions, such as head-down bed rest studies [20].

In this perspective, numerical modeling has recently proved very effective to investigate the hemodynamic behavior and the *CVS* response induced by gravity changes [21–24]. In spite of such, to the best of our knowledge, the only attempts to numerically reproduce parabolic flight effects onto *CVS* were carried out by Gerber et al. [25], who performed simulations of gravity acceleration variation from 1 g to 1.8 g and then to 0 g on a lumped parameter model of the circulation, though assuming fictitious time transitions to stabilize the model.

To fully exploit the potentialities of the computational approach, in the present study we adopt the multiscale 1D–0D mathematical model of the human *CVS* proposed in our recent work [21] to simulate the posture-depending hemodynamic response to gravity changes induced by parabolic flight. Based on this recent study on the role of body tilting onto the *CVS* response, we can speculate that the *CVS* response to gravity increase (from 0 g to 1 g and then to 1.8 g) in standing posture will likely follow a similar direction to that observed when tilting from supine to upright standing. The analysis is carried out during all phases (1 g–1.8 g–0 g–1.8 g–1 g) and postures (supine, seated and standing) typically encountered during a conventional parabolic flight. The model encompasses a 1D description of the coronary and arterial tree along with a lumped parameterization of the venous return, peripheral microcirculation and cardiopulmonary circulation. The lumped systemic compartments are organized into distinct regions (from head to legs) to account for the heterogeneous effect of gravity throughout the body. The model incorporates short-term regulation mechanisms of blood pressure (arterial baroreflex and cardiopulmonary reflex) and flow (cerebral autoregulation), aimed at controlling the heart rate, cardiac contractility, peripheral vasodilation/constriction and venous tone. A suitable pressure–area relationship [26] is included for 1D carotid and vertebral arteries to deal with very low transmural pressures elicited during 1.8 g flight phases [27–29]. Intracranial pressure (*ICP*) variation with posture and gravity is also modeled to mimic cerebrospinal fluid interplay with cerebral vessels. In addition, a model

for intrathoracic pressure (*ITP*) variation with body posture and gravity acceleration is enclosed to account for thoracic cavity compression and relaxation and their relevant effect onto central hemodynamics experienced during parabolic flights [5,30].

The aims of our analysis are: (i) to test the model outcomes with the most common hemodynamic parameters found in the literature; (ii) to study the dynamics of some crucial parameters – such as central aortic pressure behavior – not generally observed during parabolic flights due to their difficult measurement (*e.g.*, through catheterization); and (iii) to assess the transient cardiac mechano-energetic response. Finally, (iv) we discuss the role of microgravity-induced elevated *ICP* as plausible hemodynamic mechanism inducing long-term spaceflight visual impairment.

2. Material and methods

2.1. The CVS model

The multiscale model of the human circulation adopted in this work was developed and validated in our previous study on *CVS* response to posture changes [21]. The model architecture – displayed in Fig. 1 – encompasses a 1D description of the arterial tree (aorta plus large systemic and coronary arteries) linked to 0D analogs of the systemic peripheral microcirculation (arteriolar, capillary and venular) and the venous return (veins and venae cavae), organized into five separate body regions, from head to legs, as illustrated in the right panel of Fig. 1. The model equations and parameters definition are reported in the Supplementary Material.

Blood motion through 1D arteries is governed by the axisymmetric form of the Navier–Stokes equations, by assuming a flat-parabolic longitudinal velocity profile over each vessel cross-section area (details in [31]). The gravity contribution is enclosed as external forcing field within the momentum balance. A non-linear viscoelastic constitutive equation for blood pressure is included to account for arterial walls mechanical properties. Mass and total pressure conservation are imposed at arterial bifurcations, while a set of lumped characteristic impedances link each terminal 1D artery with the following 0D arterioles. The 1D aorta is directly connected to the 0D left ventricle through a lumped aortic valve model. Specific numerical boundary conditions are derived for the aorta-left ventricle coupling, at bifurcations and at each terminal artery outlet section through the method of characteristics [31]. 1D governing equations were discretized and solved numerically according to a Discontinuous Galerkin Finite Elements approach, and integrated in time employing a 2-step Runge–Kutta explicit scheme with constant time step (details in [21]).

The 0D circuital RLC compartments are modeled as a system of ordinary differential equations for mass and momentum balance, accounting for vessels hydraulic resistance (R) and blood inertia (L), and by a linear algebraic constitutive equation for blood pressure depending on vessels compliance (C). Gravity is introduced via pressure sources within extended venous compartments (*i.e.*, head, arms, legs and venae cavae) according to Stevino's law, while a specific non-linear pressure–volume relationship (Melchior et al. [32]) is introduced to deal with posture-induced elevated transmural pressures encountered in leg veins (as indicated by brown squares in Fig. 1). Arms and legs venous compartments are further equipped with a lumped model of venous valves, to prevent from reverse flow. Head veins are subjected to the action of extravascular intracranial pressure (*ICP* in Fig. 1), due to cerebrospinal fluid pressure, which is modulated with posture so that head veins transmural pressure remains negligible (details on *ICP* model implementation are addressed in Appendix A).

The 0D analog of the cardiopulmonary circulation includes a time-varying elastance and a valve model for each cardiac chamber, along with lumped pulmonary arteries and veins RC compartments, as illustrated in Fig. 1. All cardiopulmonary compartments are subjected to the action of extravascular/extrachamber intrathoracic pressure (*ITP* in Fig. 1), which varies with posture and gravity acceleration, inducing marked changes in cardiac filling and central venous pressure (*CVP*, that is the right atrial pressure). The multiscale model of the coronary circulation corresponds to the one developed by Mynard &Smolich [33]. The 0D analog of the coronary microvasculature describes the perfusion of the different myocardial layers, primarily driven by the action of extravascular intramyocardial pressure (*IMP* in Fig. 1). Further details on the coronary vasculature modeling are reported in [34].

The model includes short-term blood pressure and flow control aimed at maintaining the system homeostasis. In particular, an arterial baroreflex model is implemented – with target pressure the steady-state supine mean aortic-carotid pressure – controlling the heart chronotropic and inotropic effects, arteriolar and capillary vasodilation/constriction and venous tone (venular and venous unstressed volumes and compliances). The cardiopulmonary reflex is also enclosed, targeting the mean supine right atrial pressure (*i.e.*, *CVP*), and controlling peripheral resistances and venous tone as well. Then, a cerebral autoregulation model is added to maintain proper perfusion of brain tissues during the various phases of the parabolic flight. The cerebral autoregulation model was already present in our previous work on posture changes [21], and was included in the present study since a mechanism regulating cerebral blood flow has been proved to hold also during parabolic flight [14,35]. In the present work, to resemble typical pre-flight conditions commonly observed in parabolic flight experiments [6–19], the saturation parameters of arterial baroreflex and cardiopulmonary reflex are slightly modified with respect to passive tilting condition [21] – with new settings reported in Supplementary Table 1 of the Supplementary Material – meanwhile keeping unaltered all the parameters associated with cerebral autoregulation. The improved response of short-term regulation control can be ascribed to the challenging and not completely passive pre-flight condition, where complete absence of muscular activation and bio-chemical factors intervention cannot be excluded *a priori*. All ordinary differential equations governing 0D compartments and regulation mechanisms were integrated in time via the same 2-step Runge–Kutta explicit scheme applied to the 1D discretized governing equations (details in [21]).

To further align with typical pre-flight conditions commonly observed in parabolic flight experiments [6–19], hydraulic resistances associated with arteriolar compartments are increased by 15% with respect to [21]. In the following sub-sections, only the new modeling aspects *ad hoc* introduced to account for parabolic flight effects are presented, while the remaining components and settings of the model (including related numerical algorithms) remain as reported in our previous work [21].

2.1.1. Pressure–area relationship for carotid and vertebral 1D arteries

The hypergravity phase (about 1.8 g) of a parabolic flight elicits strong changes in the *CVS*, especially at seated and standing postures. Iwasaki et al. [27] showed that carotid mean arterial pressure can drop below 45 mmHg at 1.5 g along the longitudinal body axis, although only partial constriction of the carotid arteries occurs [28]. Linnarsson et al. [29] proved that such carotid arterial pressure drop was present even at higher ventricular rate, during exercise.

The constitutive pressure–area (p-A) relationship describing arterial walls mechanics incorporated in our *CVS* model [21] was developed by Guala et al. [31], and was validated within the range 50–120 mmHg. To deal with very low arterial pressure encountered at terminal carotid and vertebral arteries, the model by Guala et al. was extended by introducing the partial collapse hyperbolic relationship proposed by Drzewiecki et al. [26], so that the novel p-A relationship reads

$$p = B_1 + B_2 A + B_3 A^2 + B_4 A^3 - B_5 \frac{1}{\sqrt{A}} \frac{\partial Q}{\partial x} - \widehat{EI}\left(\left(\frac{A_b}{A}\right)^n - 1\right) + p_b, \quad (1)$$

where $p = p(x,t)$ is arterial transmural pressure (t is time and x is vessels axial coordinate), $A = A(x,t)$ is vessel cross-section area, $Q = Q(x,t)$ is

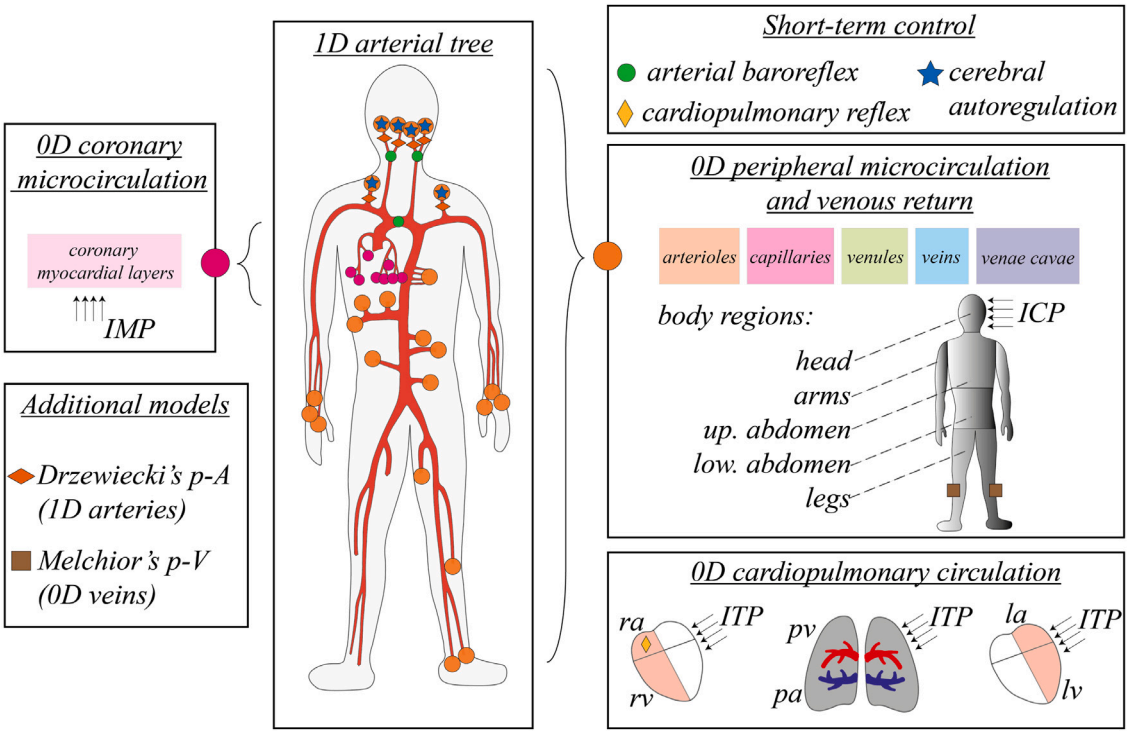

Fig. 1. Schematic illustration of the global multiscale *CVS* model (details in [21]). The red network represents 1D arteries, while the colored bands in the right panel (orange, pink, green, light and dark blue, from left to right) refer to the different compartments of the 0D systemic circulation (from arterioles to venae cavae, respectively). Orange circles indicate 1D arterial connections with distal 0D arterioles, organized by different body region (from head to legs). The 0D cardiopulmonary circulation is depicted in the bottom right panel, where *ra* and *rv* are right atrium and ventricle, *pa* and *pv* are pulmonary arteries and veins, whereas *la* and *la* are left atrium and ventricle, respectively. The 1D coronary circulation is linked to its 0D microcirculation analog through violet circles (details in [34]). *IMP*, *ICP*, and *ITP* are intramyocardial, intracranial and intrathoracic pressures, while $p-A$ and $p-V$ denote vessels pressure–area and pressure–volume relationships, respectively. (For interpretation of the references to color in this figure legend, the reader is referred to the web version of this article.)

blood flow rate, and coefficients $B_i = B_i(x)$ $(i = 1 \dots 5)$ depend on vessels mechanical properties. The remaining terms represent Drzewiecki's partial collapse model, where $\widehat{EI} = 4.14$ mmHg is the vessel flexural rigidity normalized by the lumen radius cubed, $A_b = 10$ mm^2 and $p_b = -0.64$ mmHg are buckling cross-section area and pressure (at maximum compliance), respectively, while $n = 2$ is a constant defining the degree of curvature of the p-A hyperbola. Eq. (1) applies to carotid and vertebral arteries as indicated by orange rhombs in Fig. 1.

2.1.2. Intrathoracic pressure vs. posture and gravity acceleration

Beside physiological *ITP* variation with body posture [21], Peterson et al. [30] highlighted that intrathoracic pressure is differently affected by gravity acceleration whether the subject lies supine or stands upright, due to the pushing action of the diaphragm against the thoracic cavity, as also confirmed by Norsk [5] and Videbaek & Norsk [20]. In supine posture, the diaphragm is pushed headward by the compression of the abdominal cavity with increasing gravity, thus raising *ITP* inside the thoracic cavity. Conversely, at seated or standing posture, an augmented gravity results in a releasing effect onto the thoracic cavity (*i.e.*, lower *ITP*) by pulling the diaphragm feetwards.

To take into account this diaphragm-induced effect onto the thoracic cavity state, we propose a novel *ITP* model as a function of posture (through the tilt angle α) and gravity acceleration (normalized as g/g_0, where $g_0 = 9.81$ m/s^2) by fitting data recorded in previous works (see Table 1). The new *ITP* model reads

$$ITP = -4.014 + 1.127\frac{g}{g_0} + 0.895\left(\frac{g}{g_0}\right)^2 \sin(\alpha) - 4.508\frac{g}{g_0}\sin(\alpha), \qquad (2)$$

with standard squared error SSE $= 0.21$ mmHg^2 and coefficient of determination $R^2 = 0.99$. The *ITP* time profiles computed through Eq. (2) along the parabolic flight trajectory at varying g/g_0 for both supine and seated/standing postures are reported in Fig. 2.

Table 1
Assumed value of intrathoracic pressure (*ITP*) depending on body posture (supine or seated/standing) and gravity acceleration g/g_0 (values from [5,20,30]).

Intrathoracic pressure *ITP* [mmHg]			
	0 g	1 g	1.8 g
supine	−4.1	−2.5	−2.2
seated	−4.1	−6.5	−7.2
standing	−4.1	−6.5	−7.2

2.2. Baseline postures

To comply with standard pre-flight measurements collected from the literature [6–19] and to allow for comparisons among different cardiovascular responses during the parabolic flight maneuver, baseline (pre-flight) supine, seated and standing postures are introduced. These three different pre-flight configurations (adopted as initial conditions for the parabolic flight simulations) are defined by exploiting the steady-state *CVS* configuration approached after simulated passive head-up tilt to 90° performed as described in [21] (no tilting is performed for the supine posture), assuming the new model calibration introduced in Section 2.1.

In particular, the pre-flight baseline seated posture is obtained by simulating tilt from supine to upright 90° via the following assumptions: (i) at $\alpha \neq 0$ the gravitational contribution to the momentum balance equation is neglected along the whole femoral and deep femoral arteries (arteries #45 and #46 with reference to [21]); (ii) the hydrostatic height of the 0D legs venous compartment is reduced by accounting for only half the anatomical length of the leg veins.

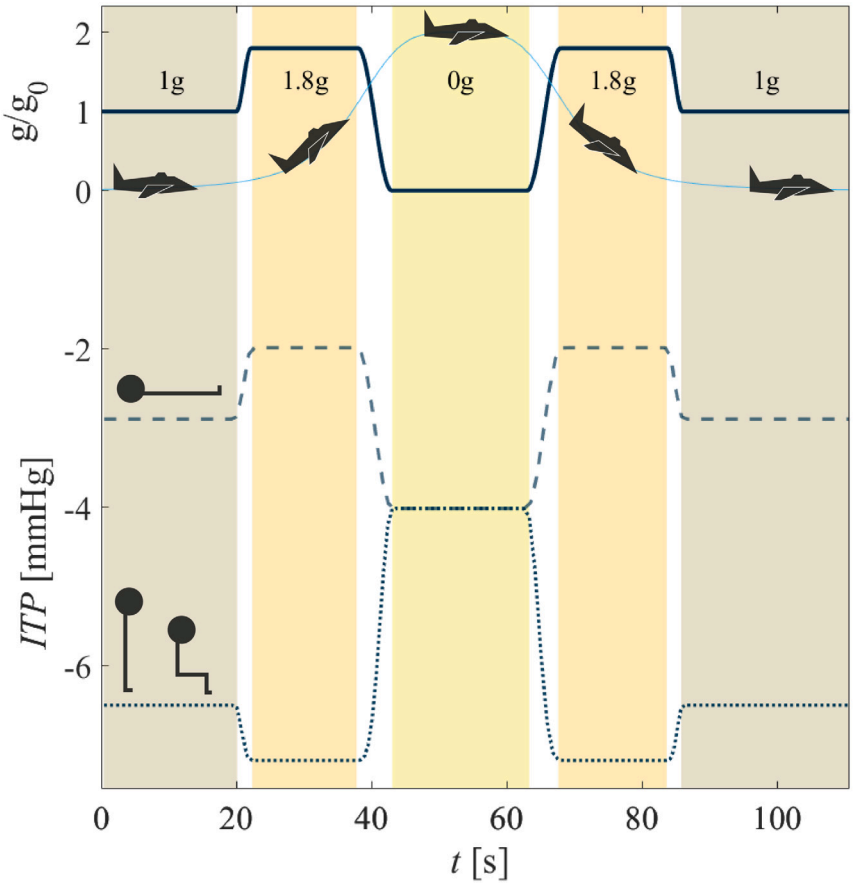

Fig. 2. Illustration of the parabolic flight time profile. On top, the parabolic flight profile is sketched together with the corresponding gravity acceleration profile g/g_0 (with $g_0 = 9.81$ m/s^2). Below, the time behavior of intrathoracic pressure *ITP* at different postures (supine: dashed line; seated and standing: dotted line) is reported.

2.3. Parabolic flight simulation

A standard parabolic flight profile is designed on the basis of the most common parabolic flight campaigns reported in the literature [6–19]. Typically, the duration of each phase of flight (hyper- and microgravity) lasts about 20 s, with fast transitions between each phase of few seconds (refer to the flight profiles reported by Mukai et al. [6] and Liu et al. [12]). The implemented g/g_0 time profile is depicted in Fig. 2, together with the corresponding sketch of the parabolic flight trajectory. Each gravity transition is modeled as a cosinusoidal function of time:

$$\frac{g}{g_0} = \left(\frac{g}{g_0}\right)_i \pm \frac{1}{2}\left[\left(\frac{g}{g_0}\right)_f - \left(\frac{g}{g_0}\right)_i\right]\cdot\left[1 \mp \cos\left(\frac{t - t_i}{\Delta t_{i-f}}\pi\right)\right], \tag{3}$$

taking the upper sign for ascending g/g_0 ramps, whereas the lower one for descending g/g_0 ramps. In Eq. (3), subscripts i and f refer to the initial and final gravity acceleration magnitude of the corresponding transition phases, respectively, with t_i and Δt_{if} being the starting time of transition and the transition phase duration, respectively. Both the pull-up (1 g–1.8 g) and pull-out (1.8 g–1 g) phases as well as the parabolic maneuver (1.8 g–0 g and subsequent 0 g–1.8 g) are performed at fixed time rate (±0.36 g/s). The duration of each gravity transition phase Δt_{i-f} (*i.e.*, $\Delta t_{1g-1.8g}$, $\Delta t_{1.8g-0g}$ and *vice versa*) is reported in Table 2, together with the time duration of each phase of flight: $T^I_{1.8g}$ and $T^{II}_{1.8g}$ for the first and second hypergravity phases, and T_{0g} for the microgravity phase, respectively.

2.4. Mechano-energetic indexes

To grasp information regarding the global *CVS* mechano-energetic balance (*i.e.*, the cardiac oxygen demand–supply ratio) during parabolic flight, we focus on the behavior of the different oxygen consumption indexes – the rate-pressure product *RPP*, the tension-time index *TTI* and the pressure–volume area *PVA* [36] – and the corresponding energy supply parameter, described by the cardiac work (or stroke work, *SW*), corresponding to the area of the left ventricle pressure–volume loop. The analyzed beat-to-beat oxygen consumption indexes are defined as:

$$RPP = p_{aor,sys} \cdot HR, \tag{4}$$

where $p_{aor,sys}$ is aortic systolic pressure;

$$TTI = p_{lv,mean} \cdot RR, \tag{5}$$

with $p_{lv,mean}$ being the mean left ventricle pressure computed over the heartbeat, while *EF* is the heartbeat duration; and

$$PVA = PE + SW, \tag{6}$$

where *PE* is left ventricle potential energy, defined as $PE = p_{lves}(V_{lves} - V_{lv}^{un})/2 - p_{lved}(V_{lved} - V_{lv}^{un})/2$, with p_{lves}, p_{lved}, V_{lves}, V_{lved} and V_{lv}^{un} being left ventricle end-systolic and end-diastolic pressures, end-systolic and end-diastolic volumes, and unstressed volume, respectively.

We also assess cardiac efficiency by means of the ejection fraction

$$EF = SV/V_{lved}, \tag{7}$$

expressing the ratio between blood volume ejected from the left ventricle (SV) and the maximum available left ventricular volume (end-diastolic volume, V_{lved}), and SW/PVA, the cardiac energy supply vs. demand ratio. To allow for the comparison between flight phases and postures, as well as with *RPP*, all these quantities are expressed per minute by multiplicating them by the heart rate *HR* (*i.e.*, SW/min=$SW \cdot HR$, PVA/min=$PVA \cdot HR$, TTI/min=$TTI \cdot HR$).

Table 2
Assumed values for the g/g_0 time profile parameters of a conventional parabolic flight. $\Delta t_{1g-1.8g}$, $\Delta t_{1.8g-0g}$, $\Delta t_{0g-1.8g}$, $\Delta t_{1.8g-1g}$ are the gravity transitions duration from 1 g to 1.8 g, from 1.8 g to 0 g, from 0 g to 1.8 g and from 1.8 g to 1 g, respectively, whereas $T^I_{1.8g}$, $T^{II}_{1.8g}$ and T_{0g} are the time durations of the first and second hypergravity and of the microgravity phases, respectively.

Param.	$\Delta t_{1g-1.8g}$	$T^I_{1.8g}$	$\Delta t_{1.8g-0g}$	T_{0g}	$\Delta t_{0g-1.8g}$	$T^{II}_{1.8g}$	$\Delta t_{1.8g-1g}$
Value [s]	2.2	15.8	5.0	20.0	5.0	15.8	2.2

3. Model validation through global hemodynamic response

The model outcomes for the most commonly measured hemodynamic parameters over each phase of the parabolic flight profile at supine, seated and standing postures [6–19] are reported in Table 3. The investigated parameters include: mean, systolic and diastolic arterial pressure (*MAP*, *SAP* and *DAP*, respectively), heart rate (*HR*), left ventricle stroke volume (*SV*), cardiac output (*CO*) and total peripheral resistance (*TPR*). We recall that, as a standard practice during *in vivo* measurements aboard of parabolic flight campaigns, all authors reported arterial pressure measurements taken at peripheral sites – commonly at the finger through non-invasive photo-plethysmography and continuous beat-to-beat recording – with concurrent or subsequent correction at heart level, by keeping the hand at same height of the heart, or via suitable pressure correction. For this reason, *MAP*, *SAP* and *DAP* in Table 3 are always referred to the model finger arterial pressure (outlet section of the 1D radial artery), with subsequent subtraction of the hydrostatic contribution associated with the vertical distance between the heart and the selected site.

Although most authors performed continuous non-invasive recording of arterial pressure and *HR*, the complete time history of the inquired hemodynamic variables was made available only by a few of them [12–14,16–18]. Furthermore, the criteria for the calculation of the single flight phase average value of a given hemodynamic parameter remains heterogeneous among the authors. Thus, following Ogoh et al. [14], we report the single-phase time average value of each parameter evaluated over the last 10 s of each phase of flight. This allows us to exclude the first and strongest fluctuations immediately past each gravity transition.

Table 3 shows that the model is capable of accurately reproducing the global hemodynamic response to parabolic flights at different postures. The largest pressure discrepancies with respect to the measured data emerge within the 1.8 g phases at seated and standing postures, probably because of the shorter duration of these flight phases – making the set of measured values more heterogeneous – and due to the arterial site where the pressure signal is detected. Indeed, even though close to the finger, the radial artery does not coincide with the typical finger cuff placement, thus inducing unavoidable slight pressure waveform mismatches which are the cause for the observed differences between computed and measured *MAP*, *SAP* and *DAP*.

The overall hemodynamic response is well captured also in the case of supine posture. We recall that the gravity term is introduced in our model only along the main body longitudinal axis (*i.e.*, along the head-feet direction), thus no direct alteration should occur at $\alpha = 0$ (supine). However, gravity does manifest its effect through intrathoracic pressure variation (by compression or expansion of the thoracic cavity on behalf of the diaphragm), triggering weak but still appreciable hemodynamic changes. Such parameters fluctuations appear to be in the same direction as those observed in the literature [5–8,10,12,13], although Bimpong-Buta et al. [7] and Liu et al. [12] were not able to prove statistical significance of their findings.

Compared with initial and final 1 g phases, the 20 s microgravity phase shows an overall hemodynamic relaxation at all postures in terms of arterial pressure and cardiac performance. Moreover, supine 1 g differs slightly from supine 0 g, as well as from seated and standing 0 g. The reason for such a mismatch is in fact the action of intrathoracic pressure: this latter approaches a similar value upon microgravity at all postures – lower than 1 g in supine posture – thus causing improved venous return and subsequent enhanced ventricular filling, together with reduction of the heart rate. The model results at 0 g seated ad standing posture align well with those discussed for the supine posture.

It is evident from Table 3 that the first and second hypergravity phases trigger the *CVS* response to a different extent. Despite keeping constant all gravity rates of variation during flight maneuvers, the drop in arterial pressure (*MAP*, *SAP* and *DAP*) is much larger for the second 1.8 g phase than during the first one, with an even stronger decrease in standing (*MAP* −26% second 1.8 g vs. −6% first 1.8 g, compared to 1 g) than seated (*MAP* −13% second 1.8 g vs. −1% first 1.8 g, compared to 1 g) posture. Meanwhile, also *SV* and *CO* fall to deeper values upon the second 1.8 g than during the first 1.8 g phase for the standing and seated postures, with corresponding *HR* reaching higher levels (standing: +39% second 1.8 g vs. +33% first 1.8 g; seated: +46% second 1.8 g vs. +34% first 1.8 g, with respect to 1 g) to compensate blood pressure dip. No evident differences emerge between first and second hypergravity phases in supine posture. Among the possible reasons for such different response to 1.8 phases, one plausible factor is the different *TPR* increment promoted by short-term regulation mechanisms (in particular arterial baroreflex and cardiopulmonary reflex): the detected rise in *TPR* goes from +4% (first 1.8 g) to −3% (second 1.8 g) for the seated posture, and from +1% (first 1.8 g) to −9% (second 1.8 g) for the standing posture, with respect to corresponding 1 g values. The weaker *TPR* response associated with the second 1.8 g phase may be due to the 20 s microgravity phase preceding the 0 g–1.8 g transition. During 0 g, *TPR* approaches an overall vasodilated state with reduction by −25% at seated and −26% at standing posture, compared to 1 g (reaching late-0 g values very similar to supine 1 g and 0 g). The fast transition from 0 g to 1.8 g (within 5 s) elicits a strong increment in *TPR*, whose rate of response is of the order of ∼10 s (Supplementary Table 1), but the resulting *TPR* reached after pull-out (0 g–1.8 g) is lower than that observed after the initial pull-up (1 g–1.8 g) phase, due to the different pre-transition (from 1 g or 0 g, respectively) *TPR* state. Therefore, the fall in blood pressure experienced during the 0 g–1.8 g transition is almost entirely contrasted by a further *HR* and ventricular contractility increase, both characterized by faster rate of response (∼3 s).

4. Results

4.1. Transient response and central aortic pressure

Through our model, we can compute the transient behavior of several hemodynamic variables over the parabolic flight maneuver, at all commonly considered postures (supine, seated and standing). In the Supplementary Material we report the transient dynamics of some meaningful hemodynamic parameters – *HR*, *CO*, *SV*, *TPR* and V_{cp}, that is cardiopulmonary compartments blood volume – during parabolic flight, and their behavior will be recalled in the following discussion. Here, we focus on the transient response of central (aortic root) mean arterial pressure (*cMAP*, see Fig. 3) due to its key-role in describing and understanding the overall functioning of the *CVS* when undergoing parabolic flight at different postures. Besides, *cMAP* is not typically investigated during parabolic flight campaigns, because of the difficult (invasive) measurement of such variable. Only Ogoh et al. [14] and Seibert et al. [19] reported data from continuous monitoring of central aortic pressure for seated subjects during parabolic flights, although in these studies *cMAP* is computed through transfer function

Table 3
Comparison between model outcomes and measured data for the most common hemodynamic parameters divided by posture and flight phase. *MAP* mean arterial pressure, *SAP* systolic arterial pressure, *DAP* diastolic arterial pressure (blood pressures always referred to finger arterial pressure corrected at heart level), *HR* heart rate, *SV* stroke volume, *CO* cardiac output, *TPR* total peripheral resistance. The model outcomes are computed by averaging the last 10 s of each flight phase (percentage variations with respect to standing 1 g values are included only when absolute ranges are not available in literature). Benchmark values are taken from [6–19] and are reported in squared brackets. Symbols help identify trends reported in the literature for the corresponding variables, with respect to their 1 g pre-flight state (≅: not clear trend, ↑: parameter increase, ↓: parameter decrease).

Posture	Parameter	**1g**	**1.8g**	**0g**	**1.8g**	**1g**
Supine	*MAP* [mmHg]	87 [73÷101]	85 [68÷98] ≅	89 [78÷96] ≅	84 [68÷95] ≅	87 [75÷95]
	SAP [mmHg]	150 [112÷144]	146 [113÷139] ≅	154 [120÷144] ≅	146 [111÷139] ≅	150 [114÷144]
	DAP [mmHg]	54 [55÷83]	54 [53÷81] ≅	54 [60÷80] ≅	53 [53÷75] ≅	54 [57÷79]
	HR [bpm]	70 [60÷89]	74 [60÷88] ≅	66 [61÷91] ≅	73 [61÷84] ≅	70 [60÷88]
	SV [ml]	76 (123%) [132%÷134%]	71 (115%) [126%÷142%] ≅	82 (133%) [125%÷151%] ≅↑	72 (116%) [124%÷138%] ≅	76 (123%) [130%÷136%]
	CO [l/min]	5.3 (109%) [106%÷108%]	5.2 (107%) [97%÷121%] ≅	5.4 (111%) [98%÷122%] ≅↑	5.2 (108%) [91%÷115%] ≅	5.3 (109%) [103%÷109%]
	TPR [mmHg min/l]	16.1 (82%) [80%÷82%]	15.9 (81%) [70%÷90%] ≅	16.4 (83%) [71%÷89%] ≅	15.9 (80%) [77%÷87%] ≅	16.2 (82%) [77%÷87%]
Seated	*MAP* [mmHg]	97 [85÷105]	96 [90÷110] ≅↓	88 [70÷101] ↓	84 [80÷105] ≅↓	97 [80÷110]
	SAP [mmHg]	158 [109÷153]	151 [110÷155] ≅↑	158 [102÷133] ≅↓	132 [110÷156] ≅	158 [125÷163]
	DAP [mmHg]	69 [69÷89]	74 [73÷99] ↑	51 [57÷79] ↓	64 [68÷92] ≅	69 [71÷89]
	HR [bpm]	74 [63÷86]	99 [74÷113] ↑	68 [62÷90] ↓	108 [74÷109] ↑	75 [67÷93]
	SV [ml]	68 (110%) [50÷111]	48 (78%) [40÷90] ↓	87 (142%) [70÷125] ↑	41 (67%) [50÷100] ↓	68 (110%) [50÷100]
	CO [l/min]	5.0 (104%) [4.0÷8.5]	4.8 (98%) [4.0÷8.9] ↓	5.9 (122%) [5.0÷9.9] ↑	4.5 (92%) [4.5÷8.9] ↓	5.0 (104%) [4.0÷8.0]
	TPR [mmHg min/l]	19.4 (98%) [11.8÷22.2]	20.1 (102%) [12.5÷25.0] ≅↑	14.8 (75%) [9.1÷16.7] ↓	18.8 (95%) [10.0÷22.2] ≅	19.4 (98%) [11.8÷22.2]
Standing	*MAP* [mmHg]	95 [90÷102]	89 [95÷105] ≅↑	87 [75÷97] ↓	70 [90÷94] ≅↓	95 [88÷98]
	SAP [mmHg]	153 [136÷154]	139 [131÷151] ≅↓	158 [127÷151] ≅↓	110 [127÷139] ≅↓	153 [139÷149]
	DAP [mmHg]	69 [72÷86]	70 [80÷90] ≅↑	50 [57÷75] ↓	54 [73÷79] ≅↓	69 [70÷82]
	HR [bpm]	79 [69÷104]	105 [82÷117] ↑	69 [60÷90] ↓	110 [80÷119] ↑	80 [73÷102]
	SV [ml]	62 (100%) [39÷77]	43 (69%) [28÷70] ↓	88 (142%) [41÷117] ↑	35 (57%) [85%÷109%] ↓	61 (99%) [97%÷105%]
	CO [l/min]	4.9 (100%) [4.3÷5.7]	4.5 (92%) [83%÷99%] ↓	6.0 (124%) [7.9÷15.1] ↑	3.9 (80%) [92%÷124%] ↓	4.9 (100%) [99%÷103%]
	TPR [mmHg min/l]	19.8 (100%) [100%]	20.0 (101%) [102%÷130%] ≅↑	14.6 (74%) [63%÷83%] ↓	17.9 (91%) [79%÷107%] ≅	19.8 (100%) [94%÷98%]

reconstruction (*e.g.*, SphygmoCor platform, AtCor medical, or similar instruments).

By observing Fig. 3 it is evident that the response of *cMAP* to parabolic flight is triggered proportionally to the body posture (*i.e.*, stronger response in going from supine to seated and, lastly, to standing posture). Despite the initial 1 g pre-flight values of *cMAP* – 93 mmHg at supine, then 98 mmHg at standing and 100 mmHg at seated posture (pressure is higher at seated than standing because of the more effective response of short-term control in relation to a lower feetwards blood migration) – the standing posture produces the strongest *cMAP* fluctuations compared to 1 g pre-flight, reaching values as low as 70 mmHg (first 1.8 g peak) and 45 mmHg (second 1.8 g peak). The marked reduction in *cMAP* registered in both 1.8 g phases at seated and standing postures is primarily due to the sudden blood migration to lower extremities, as confirmed by the corresponding reduction in V_{cp} (Supplementary Figure 5) – reduced by about −200 ml and −300 ml during first and second 1.8 g, respectively, compared to initial 1 g values, at both seated and standing postures – and consequently in *SV* (Supplementary Figure 2), dropped by −20÷−30 ml at seated and standing postures with respect to 1 g. As already highlighted in Table 3, the model response to hypergravity at seated and standing postures produces discrepancies between computed arterial pressure and the available reference data. This holds also for *cMAP* with respect to the data reported by Ogoh et al. [14] for seated subjects, during 1.8 g phases. Beside the model limitations in predicting the accurate arterial pressure response to such conditions, we should consider also the difficulties of the aortic pressure measurement performed by the authors in [14]: they did not perform a direct (*e.g.* catheterized) measurement of central aortic pressure, but the latter is obtained through transfer function reconstruction with brachial calibration, difficult to perform over a very limited time interval. During hypergravity, *HR* (Supplementary Figure 1) is raised up to 100÷110 bpm at seated and standing postures to promptly counteract the abrupt drop of *cMAP*, together with concurrent vasoconstriction of peripheral vessels (*TPR*

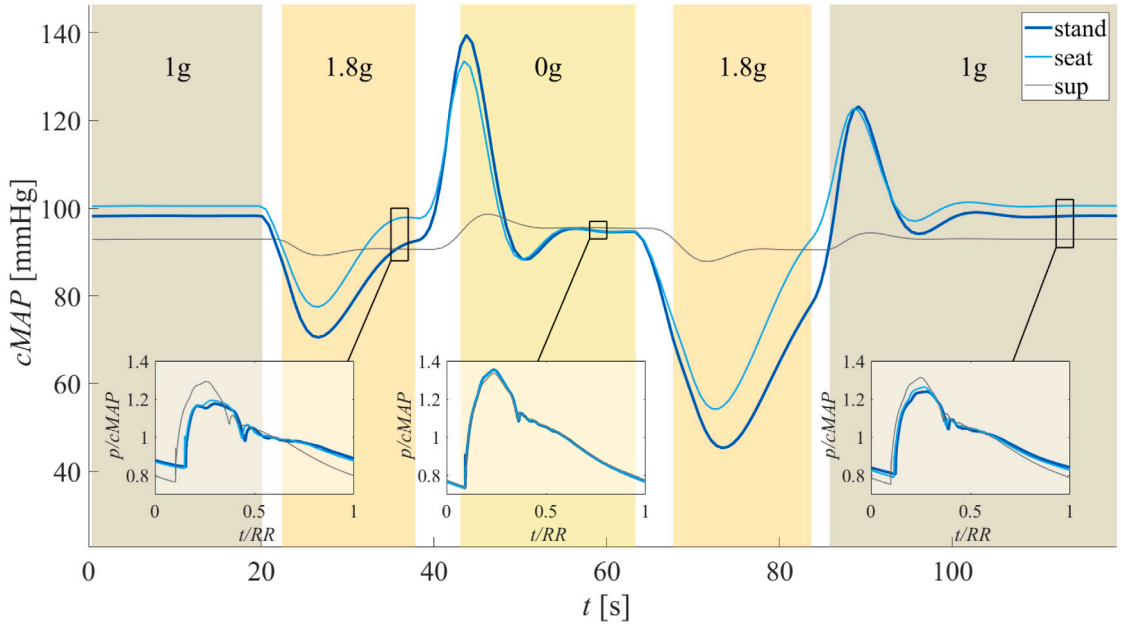

Fig. 3. Transient response of central (aortic root) mean arterial pressure (*cMAP*) to parabolic flight at different postures (gray line: supine (sup), light blue line: seated (seat), dark blue line: standing (stand)). Snapshots of the normalized aortic root pressure waveform (*p/cMAP*) – taken at each late-phase of the parabolic flight – are also reported in the insets at 1.8 g, 0 g and final 1 g, respectively, from left to right. Normalization was performed with respect to the local heartbeat duration (*EF*) and *cMAP*. (For interpretation of the references to color in this figure legend, the reader is referred to the web version of this article.)

enhanced by +10%÷+20%, see Supplementary Figure 4). As a result, during hypergravity *CO* (Supplementary Figure 3) initially drops by −22%÷−47% (first and second 1.8 g negative peaks, respectively, with respect to initial 1 g) at seated and standing postures, as also does *cMAP* (seated −23% and standing −29% at first early-1.8 g; seated −46% and standing −54% at second early-1.8 g), then both variables recover up to values slightly below (*CO*, seated −4% and standing −7% at first late-1.8 g; seated −7% and standing −15% at second late-1.8 g) or almost comparable (*cMAP*) to 1 g pre-flight conditions. During both hypergravity phases at supine posture the *CVS* model responds in a similar way but to a much lower extent compared to seated and standing, owing to the compression of the thoracic cavity on behalf of the augmented gravity acceleration. The resulting higher *ITP* participates in disadvantaging venous return to the heart, thus weakly limiting *cMAP* (−3% at both 1.8 phases, compared to 1 g), *SV* (−5 ml) and *CO* (−2%), and causing a moderate increase in *HR* (74 bpm at both 1.8 g phases vs. 70 bpm at 1 g).

The 20 s microgravity phase and the transition from previous 1.8 g phase entail a number of different responses. Given the sudden and conspicuous blood volume transfer from lower extremities to central regions (V_{cp} immediately rises by about +450 ml at seated and standing postures upon reaching 0 g from 1.8 g), *cMAP* is raised to almost 130÷140 mmHg, and so does *SV* (+30÷+35 ml at seated and standing postures, with respect to initial 1 g). Successively, following the overall systemic relaxation with *HR* reduction to values underneath pre-flight 1 g (65÷68 bpm at all postures) and peripheral vasodilation (*TPR* decreases by -37% at seated and standing postures, with respect to 1 g), near pre-flight *cMAP* and *CO* supine values are approached. However, the 0 g *CVS* overall configuration reached in late-microgravity at all postures shows fundamental differences with respect to supine 1 g pre-flight. Indeed, by complete removal of the gravity field and consequent redistribution of blood volume and pressure all over the circulation, the resulting situation should be identical among postures and in turn well comparable with supine 1 g pre-flight. Conversely, the *CVS* reaches a globally more relaxed configuration with respect to supine 1 g, with *cMAP* little increased (95 mmHg for all postures at 0 g vs. 93 mmHg at supine 1 g) together with increased *SV* (about +6 ml at 0 g supine posture and +10 ml at 0 g seated and standing postures, compared to 1 g supine) and *CO* (+2% at 0 g supine posture, about +8% at 0 g seated and standing postures, compared to 1 g supine) and reduced *HR* (65÷67 bpm for all postures at 0 g vs. 70 bpm at supine 1 g) and *TPR* (almost no variation at 0 g supine posture, about -5% at 0 g seated and standing postures, compared to 1 g supine). The enhanced cardiac filling observed even at supine posture during microgravity (0 g supine V_{cp} about +25 ml compared to 1 g) is again made possible thank to the reduced *ITP* encountered in 0 g (about −4 mmHg) compared to basal 1 g supine *ITP* (about −2.5 mmHg), allowing for reduction of *CVP* and therefore for promotion of cardiac preload [5,20,30].

The final 1 g post-flight condition is approached after the pull-out 1.8 g–1 g transition phase. As for the 1.8 g–0 g and 0 g–1.8 g transitions, also the pull-up and pull-out phases show non-symmetric responses in terms of over- and undershoots of *cMAP* (see Fig. 3) and of all other hemodynamic parameters reported in the Supplementary Material, especially at seated and standing postures. The reason for such different transient response may be linked to the lower readiness of parasympathetic short-term control response in regulating blood pressure compared to sympathetic activity. All variables eventually reach the same 1 g pre-flight condition for all simulated postures, as also evidenced in Table 3.

In Fig. 3 we also report the aortic root normalized pressure waveform (in the insets) referred to each late phase of flight. By analyzing the shape alteration of the aortic pressure waveform experienced at various postures and gravity accelerations, we grasp a number of aspects: (i) aortic pulse pressure – which is already reduced at 1 g standing and seated postures compared to supine owing to the increased *HR* and diastolic pressure associated with passive orthostatic stress (refer to [21]) – undergoes further contraction with increasing gravity from 1 g (right inset of Fig. 3) to 1.8 g (left inset) especially at seated and standing postures; (ii) entering microgravity (central inset) restores almost the same pressure waveform as in 1 g supine (albeit a slight increment in pulse pressure), and no evident difference is found among postures at this stage; (iii) by looking at the temporal instants of the diastolic minimum, systolic maximum and dicrotic notch, it emerges that parabolic flight induces a marked signal phase shifting, in particular for the standing and seated posture and during hypergravity phases. Such shifting is mainly imputable to *HR* variation, responsible for the

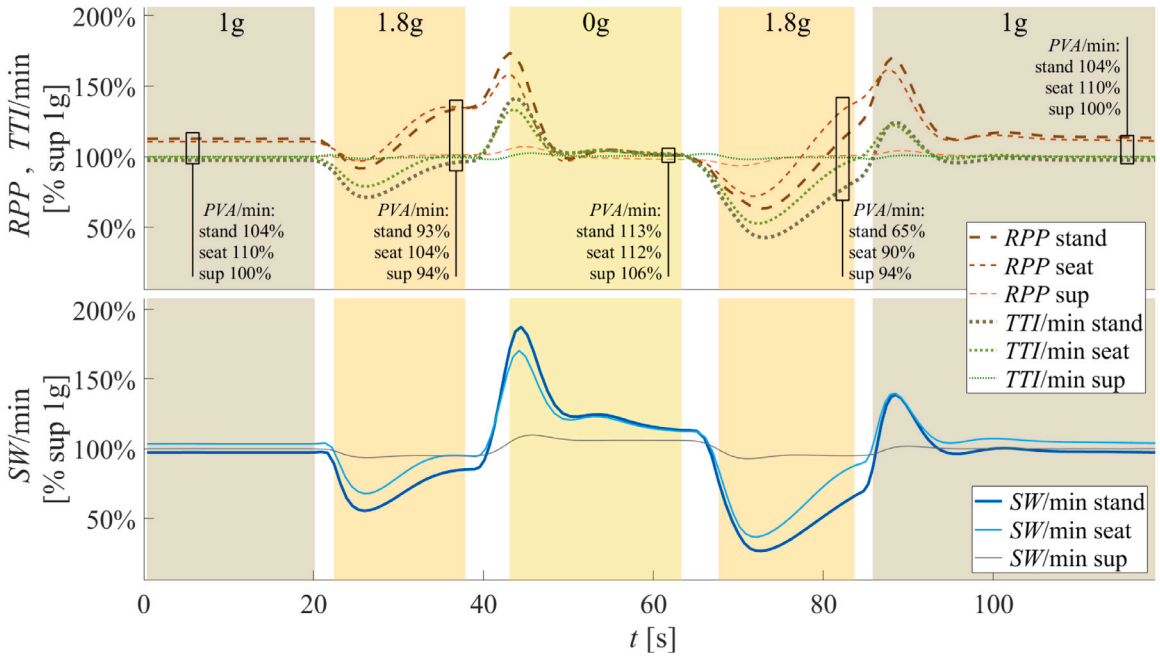

Fig. 4. Transient response of oxygen demand indexes (top panel) *RPP* (rate-pressure product: orange, dashed lines), *TTI*/min (tension-time index per minute: green, dotted lines) and *PVA*/min (pressure–volume area per minute: local values in black text) compared to left ventricle energy supply (bottom panel) *SW*/min (stroke work per minute: solid lines) during parabolic flight at different posture: supine, seating and standing (abbreviated as sup, mean and stand), from thin to thick lines, respectively. Percentage values as expressed with respect to corresponding supine 1 g states.

alteration in systolic and diastolic duration within the single heartbeat (see [21]).

4.2. Mechano-energetic analysis

In Fig. 4 we report the transient behaviors of the energy demand indexes *RPP* and *TTI*/min and the corresponding energy supply *SW*/min (all indexes are presented as percentage value of their respective 1 g supine conditions). We notice that *SW*/min at both initial 1 g standing and seated postures are similar to the corresponding supine value (97% and 103% respectively), whereas oxygen demand *RPP* is higher than the corresponding 1 g initial supine value at both seated and standing postures (110% and 112% respectively), and *TTI*/min is almost unchanged at all postures (except for a modest decrease at standing posture to 97% of supine 1 g). Successively, as the parabolic flight maneuver is initiated reaching the first 1.8 g phase, *RPP* rises up to 135% at seated and standing postures (driven by the increasing *HR* and the mildly reduced $p_{aor,sys}$), opposite to *SW*/min initially falling down to 68% (seated) and 55% (standing) - due to the *SV* and V_{cp} drop and only partially contrasted by the increasing *HR* - and then recovering to about 95% and 84% for the seated and standing postures, respectively. In this phase, *TTI*/min initially drops by -22% at seated and -29% at standing posture, compared to supine 1 g, but then recovers up to 100% and 96%, respectively. Notice that, despite its late increment, percentage *SW*/min remains lower than both *RPP* and *TTI*/min during the whole 1.8 phase, highlighting a substantial energy demand/supply unbalance. The supine posture along all the first 1.8 g phase shows very weak variations, with *SW*/min decreased to 95% and *RPP* slightly augmented to 101%, while *TTI*/min remains almost unaltered. The second 1.8 g phase following 20 s microgravity exhibits a similar overall behavior, although with further pronounced undershoots – especially at seated and standing postures – due to the sudden transition from 0 g to 1.8 g, starting from a globally much more relaxed *CVS* condition (low *HR* and *TPR* at 0 g).

The 20 s microgravity inverts the picture. After a first strong peak registered for all indexes – *SW*/min up to 170% at seated and 187% at standing posture, *RPP* to 158% at seated and 172% at standing posture, *TTI*/min to 134% at seated and 141% at standing posture – oxygen demand indexes (*RPP* and *TTI*/min) at all postures fall down to values below (*RPP*) or proximal (*TTI*/min) to the corresponding 1 g pre-flight state, and well comparable with supine 1 g pre-flight values (98%÷102% for both *RPP* and *TTI*/min), likely because of the lowered *HR*. Conversely, energy supply remains at higher levels (*SW*/min about 114% at seated and standing postures, 106% at supine posture) in late microgravity, due to the augmented ventricular filling (*SV*) promoted by the improved venous return (confirmed by the increased V_{cp} at all postures).

At the end of the parabolic flight maneuver, all indexes approaches the same 1 g pre-flight values, even though the strong variation experienced during the pull-out phase is not perfectly symmetric with respect to the pull-up phase. Again, the reason for such behavior lies in the different response of short-term control sympathetic and parasympathetic activities in regulating blood pressure.

In Fig. 4 we report also local percentage values of *PVA*/min corresponding to each late-phase of the parabolic flight. The behavior of this index of oxygen consumption is quite opposite to *RPP*, lying in between the corresponding local *TTI*/min and *SW*/min values. Indeed, *PVA*/min decreases for all postures during hypergravity phases (with respect to supine 1 g), whereas it rises in microgravity compared to 1 g supine at all postures. The reason for such behavior can be the strong dependence of *PVA*/min on *SW*/min, explaining the similar transient response of these two parameters to the parabolic flight maneuver. However, as for *TTI*/min, also *PVA*/min exhibits reduced drops (during 1.8 g phases) and rises (0 g phase) compared to *SW*/min, confirming the above mentioned energy demand–supply unbalance.

Fig. 5 illustrates the transient response to parabolic flight at different postures of the indexes of cardiac efficiency, *EF* and *SW*/*PVA*. The behavior of these two indexes is qualitatively very similar, but the information carried is two-fold. *EF* represents the emptying performance of the heart, that is how much the left ventricle succeeds in ejecting blood during systole. On the other hand, *SW*/*PVA* is an index of the cardiac energy demand–supply ratio. Both indexes drop during first hypergravity at seated and standing postures, because of the strong reduction in *SV* and *SW*/min (Fig. 4). An analog response

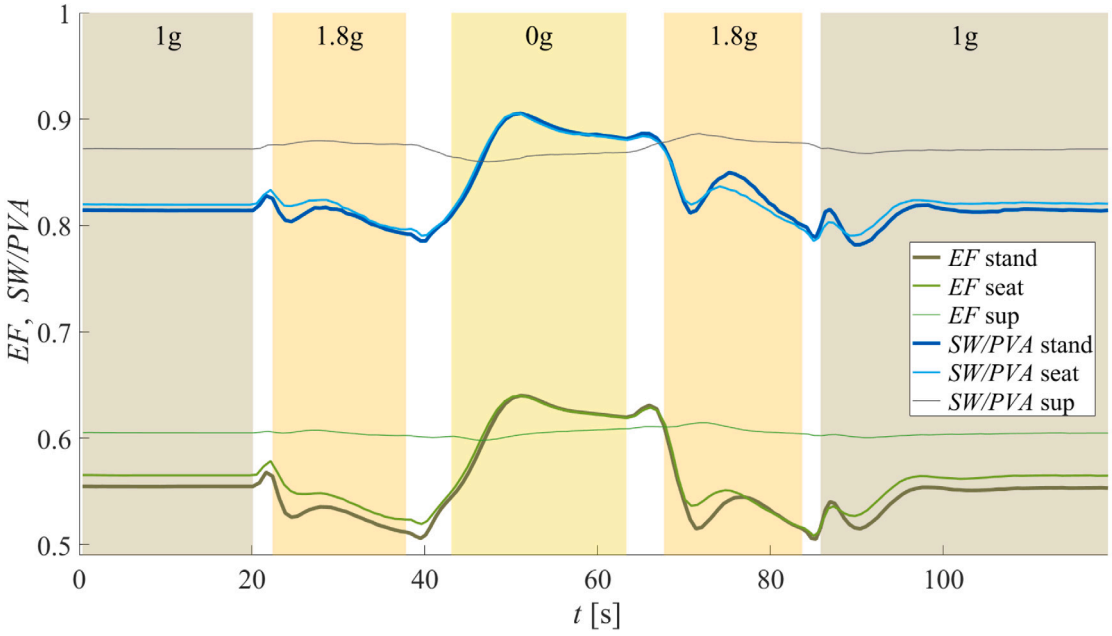

Fig. 5. Transient response of ventricular efficiency indexes *EF* (ejection fraction: lower lines) and *SW/PVA* (upper lines) during parabolic flight at supine, seated and standing postures (sup, seat and stand, from thin to thick lines, respectively).

Table 4
Ratio between areas underlying the diastolic (A_{dia}) and systolic (A_{sys}) portions of the aortic pressure waveform, evaluated during each late-phase of flight. In parenthesis, the percentage values referred to supine 1 g state are reported.

Aortic pressure waveform diastolic-to systolic A_{dia}/A_{sys}					
	1 g	1.8 g	0 g	1.8 g	1 g
supine	1.49 (100%)	1.45 (97%)	1.48 (99%)	1.48 (99%)	1.49 (100%)
seated	1.47 (99%)	1.19 (80%)	1.46 (98%)	1.10 (74%)	1.47 (99%)
standing	1.41 (95%)	1.10 (74%)	1.49 (100%)	1.05 (70%)	1.40 (94%)

of *EF* and *SW/PVA* is encountered during the second 1.8 g phase. The reduction of *SW/PVA* experienced during both hypergravity phases therefore confirms the unbalance between cardiac oxygen demand and energy supply, due to the stronger reduction of *SW*/min compared to *PVA*/min (Fig. 4). Weak variations are detected for *EF* and *SW/PVA* at supine posture. In microgravity both indexes are markedly enhanced at seated and standing postures, due to the improved *SV* and *SW* driven by the increased blood migration from lower extremities toward central regions. Thus, in 0 g the energy demand–supply unbalance is inverted with *SW*/min rising more than *PVA*/min (Fig. 4). At supine posture the behavior of *EF* and *SW/PVA* is very weakly affected during microgravity.

In addition, the cardiac energy supply vs. demand balance is assessed also through the ratio between the areas underlying the diastolic and systolic portions of the aortic pressure waveform (shown in Fig. 3), respectively, as suggested in [36]. Results, computed at each late-phase of the parabolic flight, are reported in Table 4. At standing posture, the diastolic-to-systolic area ratio decreases with increasing gravity (1.8 g phases), confirming the previously discussed energy demand–supply unbalance; conversely, the ratio recovers to near-supine values in 0 g. The picture is similar at seated posture, while very weak changes with varying gravity occur at supine posture. Unlike *SW* and *SW/PVA*, in 0 g the diastolic-to-systolic area ratio does not exceed the 1 g supine value, probably because the improved diastolic duration within the heartbeat with respect to the systolic one is compensated by the augmented systolic pressure encountered in reduced gravity (refer to the insets in Fig. 3).

5. Discussion and conclusions

In this work, we used our recently developed mathematical model [21] to study the *CVS* behavior during a typical parabolic flight profile focusing on the role of different postures. We found that both hyper- and microgravity elicit a number of cardiovascular responses mainly dictated by blood volume redistribution and short-term control activation. The largest hemodynamic alterations – in terms of aortic *MAP*, *HR*, *SV*, *CO*, *TPR* and V_{cp} – are registered at standing and seated postures, although also at supine posture some minor changes are evidenced due to the compression or relaxation of the thoracic cavity under the effect of varying gravity acceleration. Blood redistribution from central to lower regions of the body during 1.8 g phases – and *vice versa* from lower to central regions during the 0 g phase – entail prompt central pressure variation both at aortic and carotid sinus level (involved in baroreflex control), as well as cardiac pressures variation, including right atrial pressure (sensed by cardiopulmonary receptors). These changes trigger a number of system responses ranging from fast improved or decreased chronotropic and inotropic cardiac effects to successive peripheral vasoconstriction/dilation and venous tone regulation, to cope with 1.8 g and 0 g conditions, respectively. Consequently, *cMAP* is restored to near-baseline values in all late-phases of flight (late-1.8 g, late-0 g) after the strong initial fluctuations following fast gravity transitions, with the system approaching a new configuration pertaining to each phase of flight (in terms of *HR*, *SV*, *CO*, *TPR*, V_{cp}).

In addition, we focused onto the cardiac oxygen demand–supply balance during the parabolic flight maneuver, and we found that the mechano-energetic impairment between oxygen demand and supply – already present at 1 g seated and standing postures comparing

RPP and *SW*/min – is further exacerbated throughout hypergravity phases at seated and standing postures. On the contrary, this energy demand–supply unbalance is inverted (with *SW*/min overcoming *RPP* and *TTI*/min) after entering microgravity at seated and standing postures, due to the improved cardiac blood filling (and thus left ventricle *SV*) and reduced ventricular rate. These findings at seated and standing postures are further corroborated by the corresponding behavior of ventricular efficiency indexes, *i.e.*, *EF* and *SW*/*PVA*, and by the assessment of the diastolic-to-systolic area ratio of the aortic pressure waveform. On the contrary, no evident variation of oxygen demand–supply balance emerges in supine posture throughout the parabolic flight.

Coherently with the observations conducted in actual spaceflight [1–5], our model describes the size of the heart as markedly increased during early-microgravity: up to +20% in cardiac volume was reported at flight day 1, well reproduced by the model predicting +8%, +15% and +23% in cardiac chambers overall volume during late-0 g of parabolic flight at supine, seated and standing postures, respectively. This volume then decreases as the permanence in microgravity continues, along with spontaneous fluid loss (−15% at flight day 7), leading to cardiac atrophy in the absence of adequate countermeasures.

Beside the model capability of describing the global hemodynamic response to parabolic flight, a major advantage of this numerical tool is that of inquiring into the transient behavior of numerous poorly observed variables, due to their difficult and invasive measurement, though of great importance for some peculiar vascular regions (*e.g.*, ocular areas). As an example, we explored the plausible role of *ICP* in the microgravity-induced mechanisms leading to the occurrence of serious visual impairment, which may eventually lead to permanent visual acuities and morphological ocular changes [2,5,37,38]. NASA has recently synthesized these symptoms as the Spaceflight-Associated Neuro-ocular Syndrome (*SANS*), claiming that *SANS* will represent the "top health risk for long-duration spaceflight" [38]. Despite the exact etiology and pathophysiology underlying *SANS* is still unclear and widely under debate, several authors believe that *ICP* may play a crucial role [2,5,37,38]. Recent studies conducted aboard of parabolic flights [37,38] has shown that *ICP* approaches values similar to 1 g supine conditions upon entering 0 g (13 ± 2.6 mmHg). In light of this, researchers have hypothesized that the chronic mildly elevated *ICP* which the eye is subjected to during prolonged 0 g can *per se* represent a potential risk factor for *SANS* insurgence. We recall that on Earth, due to the normal circadian rhythm, *ICP* changes daily from slightly negative values at standing posture to ∼12 mmHg when lying supine (according to [39] the physiological range is 5–15 mmHg; Holmlund et al. 2017 [40] suggested a supine *ICP* of 10 mmHg, while Lawley et al. 2017 [38] proposed a supine *ICP* of about 16 mmHg).

In this context, our model has already shown good capability of predicting *ICP* variations following change of posture [21], by embedding the *ICP* vs. posture relationship proposed by Holmlund et al. [40] (Appendix A). In the present study, the *ICP* behavior during parabolic flight at different postures (*i.e.*, supine, seated and standing) is examined. Fig. 6 depicts punctual values of *CVP* (main determinant of *ICP*, according to [40]) and *ICP* at all postures referred to each late-phase of flight. We found that during both hypergravity phases *CVP* and *ICP* fall even more at standing and seated postures with respect to 1 g (since *ITP* drops from −6.5 mmHg to −7.2 mmHg), while supine values do not change significantly. Upon approaching late-0 g, *CVP* and *ICP* reaches similar values for all postures, which are in turn slightly below the corresponding 1 g supine values - *CVP*: 6.6 mmHg at supine 0 g vs. 7 mmHg at supine 1 g; *ICP*: 9.6 mmHg at supine 0 g vs. 10 mmHg at supine 1 g - in line with data reported by Lawley et al. [38]. Therefore, our model confirms the mildly-elevated levels of *ICP* (though not to a pathological extent) encountered in microgravity at all postures. As believed by researchers, the prolonged maintenance of such levels of *ICP* during long-term missions may contribute to the occurrence detrimental consequences for the ocular apparatus, albeit further investigation is needed on this aspect. The implementation of a model for intraocular pressure (*IOP*) response to change of posture and gravity acceleration – including the *IOP-ICP* interplay (translaminar pressure) in determining ocular morphological changes – is needed to provide further insights into *SANS* insurgence in microgravity.

In conclusion, the present model lacks of muscular intervention mechanisms, which may play a role in enhancing blood pumping from lower extremities especially during hypergravity phases, where complete absence of muscular contraction cannot be excluded during *in vivo* measurements. Also, additional non-linear mechanisms as well as metabolic regulation of blood pressure and flow possibly involved in such a stressing condition (1.8 g) were not considered in this study. Nevertheless, the model showed good capability of reproducing known global hemodynamics response to parabolic flight at different postures, and can represent a powerful tool of investigation for hemodynamic variables poorly observed in short-term microgravity owing to their difficult – and often invasive – measurement. Moreover, the analysis of cardiac energy demand–supply parameters during parabolic flight helped shedding light onto different mechanisms affecting central and global hemodynamics upon entering short-term hyper- and microgravity environments. The model therefore reveals promising potentialities for future aerospace applications, ranging from short-term microgravity exposure to a better implementation of in-flight countermeasures.

CRediT authorship contribution statement

Matteo Fois: Conceived and designed the research, Performed the numerical simulations, Writing – original draft, Prepared the figures, Analyzed and interpreted the results, Writing – review & editing. **Luca Ridolfi:** Conceived and designed the research, Analyzed and interpreted the results, Writing – review & editing. **Stefania Scarsoglio:** Conceived and designed the research, Analyzed and interpreted the results, Writing – review & editing.

Declaration of competing interest

The authors declare that they have no known competing financial interests or personal relationships that could have appeared to influence the work reported in this paper.

Data availability statement

The raw data supporting the conclusions of this article will be made available by the authors upon request, without undue reservation.

Acknowledgment

All authors approved the version of the manuscript to be published.

Appendix A

At supine posture, *ICP* is taken as large as 10 mmHg. As proposed in [40], by taking the difference between Davson's equation for tilted and supine posture, the relation governing *ICP* with body posture is obtained:

$$ICP_{tilt} = ICP_{sup} + CVP_{tilt} - CVP_{sup} - \Delta p^{h}_{H-ra}\,, \tag{A.1}$$

where Δp^{h}_{H-ra} is the head-right atrium hydrostatic pressure difference, determined according to Stevino's law as $\Delta p^{h}_{H-ra} = \rho g \Delta h_{H-ra} \sin\alpha$, with Δh_{H-ra} the vertical anatomical distance between the head and the right atrium, while α is the tilt angle.

To account for jugular vein collapsibility, only the gravity gradient associated with the fluid column extending from the head to the jugular vein point of collapse at zero transmural pressure – that is Δh_{H-jv} – is considered (here represented simply by Δh_H, assuming the jugular

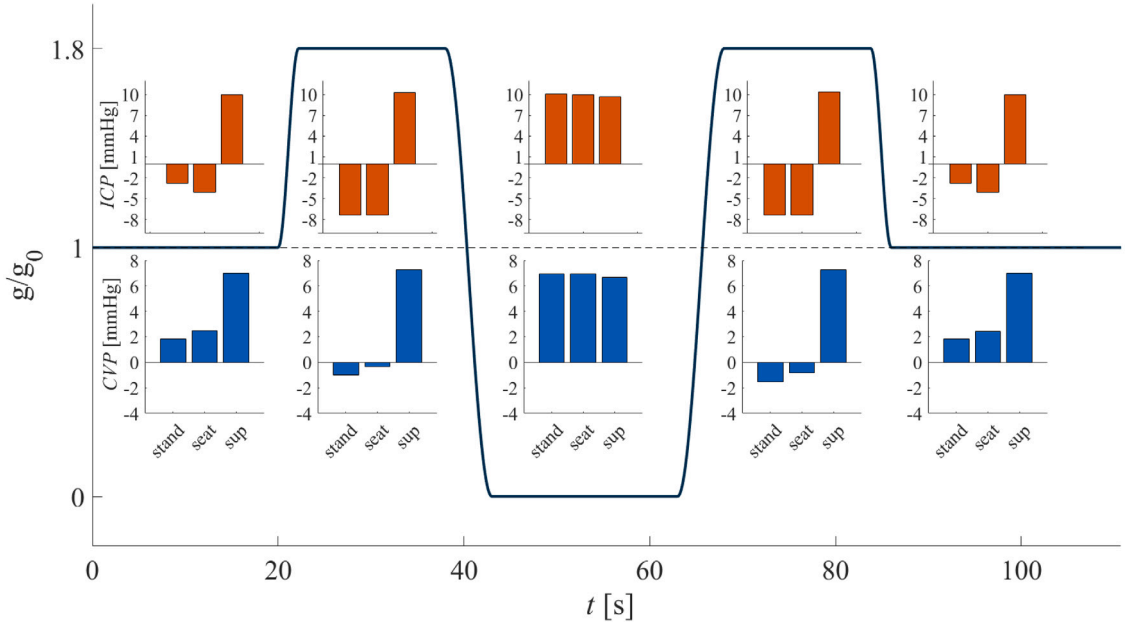

Fig. 6. Punctual late-phase values of central venous pressure (*CVP*, blue bars) and intracranial pressure (*ICP*, orange bars) during parabolic flight at different postures: standing, seated and supine (abbreviated as stand, seat and sup, respectively) from left to right in the bar charts. (For interpretation of the references to color in this figure legend, the reader is referred to the web version of this article.)

vein as corresponding to the superior vena cava compartment). The new relation implemented for tilt angles $\alpha \geq \alpha_{collapse}$ reads

$$ICP_{tilt} = ICP_{sup} - CVP_{sup} - \Delta p^{h}_{H-jv}, \tag{A.2}$$

where $\alpha_{collapse}$ is the angle for which superior vena cava pressure $p_{svc} \leq 0$. Intracranial pressure has been introduced only for cerebral veins. More detailed information about the cerebrovascular system model are provided in our previous work [21].

Appendix B. Supplementary material

Supplementary material related to this article can be found online at https://doi.org/10.1016/j.actaastro.2022.08.018. In the online Supplementary Material, detailed model's equations and parameter definitions are provided. In addition, Supplementary Table 1 reports baroreflex and cardiopulmonary reflex modeling parameters, while Supplementary Figure 1–5 illustrate the time response of additional hemodynamic variables (*HR*, *SV*, *CO*, *TPR*, V_{cp}) to parabolic flight at different postures.

References

[1] G. Clément, Fundamentals of Space Medicine, Vol. 23, Springer Science & Business Media, 2011, http://dx.doi.org/10.1007/978-1-4419-9905-4.
[2] L.R. Young, J.P. Sutton, Handbook of Bioastronautics, Springer, 2021, http://dx.doi.org/10.1007/978-3-319-12191-8.
[3] H.-C. Gunga, V.W. von Ahlefeld, H.-J.A. Coriolano, A. Werner, U. Hoffmann, Cardiovascular System, Red Blood Cells, and Oxygen Transport in Microgravity, Springer, 2016, http://dx.doi.org/10.1007/978-3-319-33226-0.
[4] P. Norsk, A. Asmar, M. Damgaard, N.J. Christensen, Fluid shifts, vasodilatation and ambulatory blood pressure reduction during long duration spaceflight, J. Physiol. 593 (3) (2015) 573–584, http://dx.doi.org/10.1113/jphysiol.2014.284869.
[5] P. Norsk, Adaptation of the cardiovascular system to weightlessness: surprises, paradoxes and implications for deep space missions, Acta Physiol. 228 (3) (2020) e13434, http://dx.doi.org/10.1111/apha.13434.
[6] C.N. Mukai, C.M. Lathers, J.B. Charles, B.S. Bennett, M. Igarashi, S. Patel, Acute hemodynamic responses to weightlessness during parabolic flight, J. Clin. Pharmacol. 31 (10) (1991) 993–1000, http://dx.doi.org/10.1002/j.1552-4604.1991.tb03662.x.
[7] N.-Y. Bimpong-Buta, J.M. Muessig, T. Knost, M. Masyuk, S. Binneboessel, A.M. Nia, M. Kelm, C. Jung, Comprehensive analysis of macrocirculation and microcirculation in microgravity during parabolic flights, Front. Physiol. (2020) 960, http://dx.doi.org/10.3389/fphys.2020.00960.
[8] L.G. Petersen, M. Damgaard, J.C. Petersen, P. Norsk, Mechanisms of increase in cardiac output during acute weightlessness in humans, J. Appl. Physiol. 111 (2) (2011) 407–411, http://dx.doi.org/10.1152/japplphysiol.01188.2010.
[9] E.G. Caiani, L. Weinert, R. Lang, P. Vaida, The role of echocardiography in the assessment of cardiac function in weightlessness—Our experience during parabolic flights, Respir. Physiol. Neurobiol. 169 (2009) S6–S9, http://dx.doi.org/10.1016/j.resp.2009.07.007.
[10] F. Beckers, B. Seps, D. Ramaekers, B. Verheyden, A. Aubert, Parasympathetic heart rate modulation during parabolic flights, Eur. J. Appl. Physiol. 90 (1) (2003) 83–91, http://dx.doi.org/10.1007/s00421-003-0854-y.
[11] U. Limper, P. Gauger, L.E. Beck, Upright cardiac output measurements in the transition to weightlessness during parabolic flights, Aviat. Space Environ. Med. 82 (4) (2011) 448–454, http://dx.doi.org/10.3357/ASEM.2883.2011.
[12] J. Liu, B. Verheyden, F. Beckers, A.E. Aubert, Haemodynamic adaptation during sudden gravity transitions, Eur. J. Appl. Physiol. 112 (1) (2012) 79–89, http://dx.doi.org/10.1007/s00421-011-1956-6.
[13] B. Pump, R. Videbæk, A. Gabrielsen, P. Norsk, Arterial pressure in humans during weightlessness induced by parabolic flights, J. Appl. Physiol. 87 (3) (1999) 928–932, http://dx.doi.org/10.1152/jappl.1999.87.3.928.
[14] S. Ogoh, A. Hirasawa, P.B. Raven, T. Rebuffat, P. Denise, R. Lericollais, J. Sugawara, H. Normand, Effect of an acute increase in central blood volume on cerebral hemodynamics, Am. J. Physiol. Regul. Integr. Comp. Physiol. 309 (8) (2015) R902–R911, http://dx.doi.org/10.1152/ajpregu.00137.2015.
[15] T.T. Schlegel, T.E. Brown, S.J. Wood, E.W. Benavides, R.L. Bondar, F. Stein, P. Moradshahi, D.L. Harm, J.M. Fritsch-Yelle, P.A. Low, Orthostatic intolerance and motion sickness after parabolic flight, J. Appl. Physiol. 90 (1) (2001) 67–82, http://dx.doi.org/10.1152/jappl.2001.90.1.67.
[16] T.T. Schlegel, E.W. Benavides, D.C. Barker, T.E. Brown, D.L. Harm, S.J. DeSilva, P.A. Low, Cardiovascular and valsalva responses during parabolic flight, J. Appl. Physiol. 85 (5) (1998) 1957–1965, http://dx.doi.org/10.1152/jappl.1998.85.5.1957.
[17] D. Widjaja, S. Vandeput, S. Van Huffel, A.E. Aubert, Cardiovascular autonomic adaptation in lunar and martian gravity during parabolic flight, Eur. J. Appl. Physiol. 115 (6) (2015) 1205–1218, http://dx.doi.org/10.1007/s00421-015-3118-8.
[18] P. Beck, J. Tank, P. Gauger, L.E. Beck, H. Zirngibl, J. Jordan, U. Limper, Modeling human orthostatic responses on the moon and on mars, Clin. Auton. Res. 28 (3) (2018) 325–332, http://dx.doi.org/10.1007/s10286-018-0527-x.
[19] F.S. Seibert, F. Bernhard, U. Stervbo, S. Vairavanathan, F. Bauer, B. Rohn, N. Pagonas, N. Babel, J. Jankowski, T.H. Westhoff, The effect of microgravity on central aortic blood pressure, Am. J. Hypertens. 31 (11) (2018) 1183–1189, http://dx.doi.org/10.1093/ajh/hpy119.
[20] R. Videbaek, P. Norsk, Atrial distension in humans during microgravity induced by parabolic flights, J. Appl. Physiol. 83 (6) (1997) 1862–1866, http://dx.doi.org/10.1152/jappl.1997.83.6.1862.
[21] M. Fois, S.V. Maule, M. Giudici, M. Valente, L. Ridolfi, S. Scarsoglio, Cardiovascular response to posture changes: Multiscale modeling and in vivo validation

during head-up tilt, Front. Physiol. 13 (2022) http://dx.doi.org/10.3389/fphys.2022.826989.
[22] A.D. Artiles, T. Heldt, L.R. Young, Effects of artificial gravity on the cardiovascular system: computational approach, Acta Astronaut. 126 (2016) 395–410, http://dx.doi.org/10.1016/j.actaastro.2016.05.005.
[23] R.S. Whittle, A. Diaz-Artiles, Modeling individual differences in cardiovascular response to gravitational stress using a sensitivity analysis, J. Appl. Physiol. 130 (6) (2021) 1983–2001, http://dx.doi.org/10.1152/japplphysiol.00727.2020.
[24] C. Gallo, L. Ridolfi, S. Scarsoglio, Cardiovascular deconditioning during long-term spaceflight through multiscale modeling, Npj Microgravity 6 (1) (2020) 1–14, http://dx.doi.org/10.1038/s41526-020-00117-5.
[25] B. Gerber, J.-L. Singh, Y. Zhang, W. Liou, A computer simulation of short-term adaptations of cardiovascular hemodynamics in microgravity, Comput. Biol. Med. 102 (2018) 86–94, http://dx.doi.org/10.1016/j.compbiomed.2018.09.014.
[26] G. Drzewiecki, S. Field, I. Moubarak, J.K.-J. Li, Vessel growth and collapsible pressure-area relationship, Am. J. Physiol. Heart Circul. Physiol. 273 (4) (1997) H2030–H2043, http://dx.doi.org/10.1152/ajpheart.1997.273.4.H2030.
[27] K.i. Iwasaki, Y. Ogawa, K. Aoki, R. Yanagida, Cerebral circulation during mild+Gz hypergravity by short-arm human centrifuge, J. Appl. Physiol. 112 (2) (2012) 266–271, http://dx.doi.org/10.1152/japplphysiol.01232.2011.
[28] C. Leguy, P. Beck, P. Gauger, L. Beck, U. Limper, Carotid arterial wall dynamics during gravity changes on partial-G parabolic flights, Microgravity Sci. Technol. 26 (2) (2014) 111–117, http://dx.doi.org/10.1007/s12217-014-9381-1.
[29] D. Linnarsson, C. Sundberg, B. Tedner, Y. Haruna, J. Karemaker, G. Antonutto, P. Di Prampero, Blood pressure and heart rate responses to sudden changes of gravity during exercise, Am. J. Physiol. Heart Circul. Physiol. 270 (6) (1996) H2132–H2142, http://dx.doi.org/10.1152/ajpheart.1996.270.6.H2132.
[30] K. Peterson, E.T. Ozawa, G.M. Pantalos, M.K. Sharp, Numerical simulation of the influence of gravity and posture on cardiac performance, Ann. Biomed. Eng. 30 (2) (2002) 247–259, http://dx.doi.org/10.1114/1.1451075.
[31] A. Guala, C. Camporeale, F. Tosello, C. Canuto, L. Ridolfi, Modelling and subject-specific validation of the heart-arterial tree system, Ann. Biomed. Eng. 43 (1) (2015) 222–237, http://dx.doi.org/10.1007/s10439-014-1163-9.
[32] F. Melchior, R. Srinivasan, P. Thullier, J. Clere, Simulation of cardiovascular response to lower body negative pressure from 0 to-40 mmHg, J. Appl. Physiol. 77 (2) (1994) 630–640, http://dx.doi.org/10.1152/jappl.1994.77.2.630.
[33] J. Mynard, J. Smolich, One-dimensional haemodynamic modeling and wave dynamics in the entire adult circulation, Ann. Biomed. Eng. 43 (6) (2015) 1443–1460, http://dx.doi.org/10.1007/s10439-015-1313-8.
[34] A. Saglietto, M. Fois, L. Ridolfi, G.M. De Ferrari, M. Anselmino, S. Scarsoglio, A computational analysis of atrial fibrillation effects on coronary perfusion across the different myocardial layers, Sci. Rep. 12 (1) (2022) 1–9, http://dx.doi.org/10.1038/s41526-020-00117-5.
[35] T. Klein, P. Wollseiffen, M. Sanders, J. Claassen, H. Carnahan, V. Abeln, T. Vogt, H.K. Strüder, S. Schneider, The influence of microgravity on cerebral blood flow and electrocortical activity, Exp. Brain Res. 237 (4) (2019) 1057–1062, http://dx.doi.org/10.1007/s00221-019-05490-6.
[36] N. Westerhof, N. Stergiopulos, M.I. Noble, B.E. Westerhof, Cardiac oxygen consumption and hemodynamics, in: Snapshots of Hemodynamics, Springer, 2010, pp. 129–134, http://dx.doi.org/10.1007/978-1-4419-6363-5.
[37] L.-F. Zhang, A.R. Hargens, Spaceflight-induced intracranial hypertension and visual impairment: pathophysiology and countermeasures, Physiol. Rev. 98 (1) (2018) 59–87, http://dx.doi.org/10.1152/physrev.00017.2016.
[38] J.S. Lawley, L.G. Petersen, E.J. Howden, S. Sarma, W.K. Cornwell, R. Zhang, L.A. Whitworth, M.A. Williams, B.D. Levine, Effect of gravity and microgravity on intracranial pressure, J. Physiol. 595 (6) (2017) 2115–2127, http://dx.doi.org/10.1113/JP273557.
[39] A. Tameem, H. Krovvidi, Cerebral physiology, Continuing Educ. Anaesth. Crit. Care Pain 13 (4) (2013) 113–118, http://dx.doi.org/10.1093/bjaceaccp/mkt001.
[40] P. Holmlund, A. Eklund, L. Koskinen, E. Johansson, N. Sundström, J. Malm, S. Qvarlander, Venous collapse regulates intracranial pressure in upright body positions, Am. J. Physiol. Regul. Integr. Comp. Physiol. 314 (3) (2018) R377–R385, http://dx.doi.org/10.1152/ajpregu.00291.2017.